Steady State Free Convection in an Unconfined Geothermal Reservoir

PING CHENG

Department of Mechanical Engineering, University of Hawaii, Honolulu, Hawaii 96822

K. H. LAU

Hilo College, University of Hawaii, Hilo, Hawaii 96720

The problem of steady state free convection in an unconfined aquifer bounded by ocean on the sides with geothermal heating from below is investigated in this paper. The governing nonlinear partial differential equations with nonlinear boundary conditions are approximated by a set of linear subproblems on the basis of perturbation method. The equations for the zero- and first-order approximations are of the elliptic type that can be solved numerically by the finite difference method. Numerical results, accurate to the first-order approximations, are obtained for temperature, pressure, and stream function as well as for the shape of the water table. The influence of the location and the size of the heat source as well as various parameters on heat transfer and fluid flow characteristics in a rectangular geothermal aquifer is discussed.

Over the past two decades much work has been done on convective heat transfer in a porous medium. *Horton and Rogers* [1945] studied the criterion for the onset of free convection in a porous medium. This was followed by a series of papers by *Lapwood* [1948], *Wooding* [1960], and *Katto and Masuoka* [1967] on the same topics.

In recent years the utilization of geothermal energy for power production has stimulated further interest in the study of heat transfer and fluid flow characteristics in geothermal reservoirs. *Wooding* [1957] obtained a numerical solution for the prediction of temperature distribution in a two-dimensional geothermal reservoir at Wairakai, New Zealand. *Donaldson* [1962] considered steady state free convection in a two-dimensional porous medium bounded by isothermal horizontal impermeable walls. The effects of a nonisothermal wall on free convection were considered by *Elder* [1967*a*, *b*]. The related problem of combined free and forced convection in a porous medium was treated by *Prats* [1966] as well as by *Combarous and Bia* [1971]. The three-dimensional problem of free convection in a porous medium inside a rectangular enclosure was studied by *Chan et al.* [1970], *Holst and Aziz* [1972*a*, *b*], and *Bories and Combarnous* [1973]. The more complicated problem of circulation patterns of groundwater affected by geothermal heating was considered by *Henry and Kohout* [1973] in their study on waste disposal. All of the preceding studies concern a porous medium bounded by impermeable walls that are applicable to confined geothermal reservoirs.

For islands of volcanic origin, aquifers are likely to be unconfined at the top. Its volcanic origin suggests that magma chambers may be present, and therefore a large source of heat may be found at a relatively shallow depth. Furthermore, the porosity of the volcanic rock permits free flow of water from the ocean into the island and thus provides a source of heat-carrying fluid. Consequently, a volcanic island may be a potential site for geothermal power plants. Thus the study of heat transfer and fluid flow characteristics in an unconfined aquifer on volcanic islands is of fundamental and practical interest.

A realistic simulation of volcanic islands as geothermal reservoirs must take into consideration the anisotropic property of rock formation, the irregular geometry of boundaries, the recharging of freshwater at the water table, and the interaction of freshwater and salt water. The mathematical solution to the realistic situation is thus a formidable task. As a first step in solving a more physically realistic problem (Figure 1, top) we shall neglect the rainfall (i.e., assuming a desert island) and idealize the geothermal reservoir as a two-dimensional isotropic and homogeneous porous medium bounded on the bottom by a horizontal impermeable surface and on the vertical sides by the ocean (Figure 1, bottom). The shape of the water table is not known a priori and must be determined from the solution. The nonlinear governing equations and nonlinear boundary conditions are approximated by a set of linear subproblems on the basis of perturbation analysis. Numerical results accurate to the first-order approximation are obtained for temperature, pressure, and stream function. The effect of nonisothermal geothermal heating on the upwelling of the water table is predicted.

Governing Equations and Boundary Conditions

As was discussed earlier, the mathematical formulation of the problem will be simplified considerably if the following assumptions are made: (1) the flow field is steady and two-dimensional, (2) the temperature of the fluid is everywhere below boiling for the pressure at that depth, (3) the convective fluid and the porous medium are everywhere in local thermodynamic equilibrium, i.e., temperature of the fluid is the same as that of the porous medium, (4) there is no accretion at the free surface, (5) fluid properties such as thermal conductivity, specific heat, kinematic viscosity, and permeability are assumed to be constant, (6) the ocean is at rest; i.e., the effects of tides are neglected, and (7) Boussinesq approximation is employed; i.e., density is assumed to be constant except in the buoyancy force term.

With these approximations the governing equations are given by

$$\operatorname{div} \mathbf{v} = 0 \tag{1}$$

$$\mathbf{v} = -\frac{k}{\mu}(\nabla p + \rho \mathbf{g}) \tag{2}$$

$$\frac{\rho}{\rho_*} = 1 - \beta(T - T_*) \tag{3}$$

$$\mathbf{v} \cdot \nabla T = \alpha \nabla^2 T \tag{4}$$

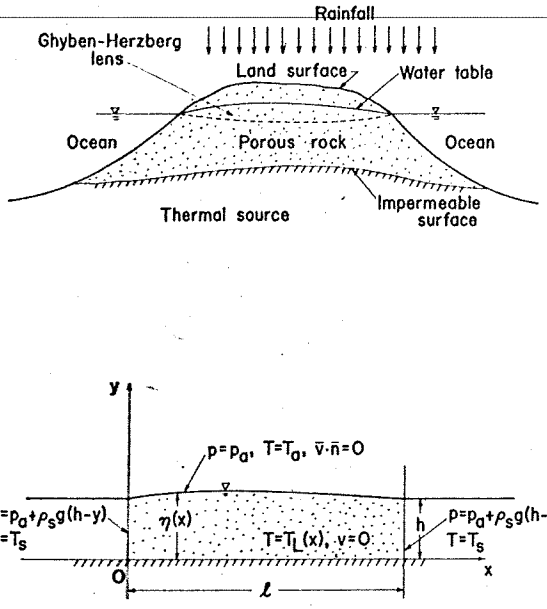

Fig. 1. (Top) An unconfined aquifer with thermal source. (Bottom) Idealized model of a geothermal reservoir.

where v, ρ, μ, and β are the macroscopic velocity vector, density, viscosity, and the thermal expansion coefficient of the fluid, p is the pressure, T is the temperature, g is the gravitational acceleration, k is the permeability of the saturated porous medium, and $\alpha = k_m/(\rho C_p)_f$ is the equivalent thermal diffusivity, k_m denoting the thermal conductivity of the saturated porous medium and $(\rho C_p)_f$ the density and specific heat of the fluid. The subscript s in (3) denotes the condition in the ocean.

The boundary conditions along the ocean are given by

$$p(0, y) = p_a + \rho_s g(h - y) \tag{5}$$

$$p(l, y) = p_a + \rho_s g(h - y) \tag{6}$$

$$T(0, y) = T_s \tag{7}$$

$$T(l, y) = T_s \tag{8}$$

Along the impermeable surface the boundary conditions are

$$v(x, 0) = 0 \tag{9}$$

$$T(x, 0) = T_L(x) \tag{10}$$

where $T_L(x)$ is prescribed. Along the free surface the boundary conditions are

$$\mathbf{v}\cdot\mathbf{n}(x, \eta) = 0 \tag{11}$$

$$p(x, \eta) = P_a \tag{12}$$

$$T(x, \eta) = T_a \tag{13}$$

where $y = \eta(x)$ is the shape of the free surface, which is not known a priori, and n is the unit vector normal to the free surface, which is given by $\mathbf{n} = \nabla F/|\nabla F|$, $F(x, y) \equiv y - \eta(x) = 0$ denoting the equation for the free surface.

With the aid of (2) and (3), boundary condition (9) can be rewritten in terms of p to give

$$\frac{\partial p}{\partial y}(x, 0) = -\rho_s g[1 - \beta(T_L - T_s)] \tag{14}$$

whereas boundary condition (11) can be rewritten as

$$\frac{\partial \eta}{\partial x}\frac{\partial p}{\partial x}(x, \eta) - \left\{\frac{\partial p}{\partial y}(x, \eta) + \rho_s g[1 - \beta(T_a - T_s)]\right\} = 0 \tag{15}$$

where (15) is the nonlinear boundary condition at the free surface.

Since boundary conditions are now in terms of p and T, we shall eliminate u, v, and ρ from (1) through (4) and express the resultant equations in terms of p and T. Thus we have

$$\frac{\partial^2 p}{\partial x^2} + \frac{\partial^2 p}{\partial y^2} = \rho_s g\beta \frac{\partial T}{\partial y} \tag{16}$$

$$\frac{\partial^2 T}{\partial x^2} + \frac{\partial^2 T}{\partial y^2} + \frac{K}{\mu\alpha}\left[\frac{\partial p}{\partial x}\frac{\partial T}{\partial x} + \frac{\partial p}{\partial y}\frac{\partial T}{\partial y} + \rho_s g[1 - \beta(T - T_s)]\frac{\partial T}{\partial y}\right] = 0 \tag{17}$$

We now express (16) and (17) with boundary conditions (5)–(8), (10), and (12)–(15) in dimensionless form. For this purpose we introduce the following dimensionless variables:

$$P \equiv \frac{p - p_a}{\rho_s g h} \qquad \Theta \equiv \frac{T - T_s}{T_c - T_s}$$

$$n \equiv \frac{\eta}{h} \qquad X \equiv \frac{x}{h} \qquad Y \equiv \frac{y}{h} \qquad L \equiv \frac{l}{h} \tag{18}$$

where T_c is the maximum temperature of the impermeable surface.

The governing equations in terms of these dimensionless variables are given by

$$\frac{\partial^2 P}{\partial X^2} + \frac{\partial^2 P}{\partial Y^2} = \epsilon\frac{\partial \theta}{\partial Y} \tag{19}$$

and

$$\frac{\partial^2 \Theta}{\partial X^2} + \frac{\partial^2 \Theta}{\partial Y^2} + D\left[\frac{\partial P}{\partial X}\frac{\partial \Theta}{\partial X} + \frac{\partial P}{\partial Y}\frac{\partial \Theta}{\partial Y} + [1 - \epsilon\Theta]\frac{\partial \Theta}{\partial Y}\right] = 0 \tag{20}$$

where $\epsilon \equiv \beta(T_c - T_s)$ and $D \equiv \rho_s K g h/\alpha\mu$ is called the discharge number, which is a measure of the imposed pressure forces to the viscous force. Boundary conditions in terms of dimensionless variables are rearranged to give

$$P(0, Y) = 1 - Y \tag{21a}$$

$$P(L, Y) = 1 - Y \tag{21b}$$

$$\frac{\partial P}{\partial Y}(X, 0) = -1 + \epsilon\Theta_L(X) \tag{21c}$$

$$\frac{\partial n}{\partial X}\frac{\partial P}{\partial X}(X, n) - \left[\frac{\partial P}{\partial Y}(X, n) + 1 - \epsilon\Theta_a\right] = 0 \tag{21d}$$

$$P(X, n) = 0 \tag{21e}$$

$$\Theta(0, Y) = 0 \tag{22a}$$

$$\Theta(L, Y) = 0 \tag{22b}$$

$$\Theta(X, 0) = \Theta_L(X) \tag{22c}$$

$$\Theta(X, n) = \Theta_a \tag{22d}$$

where $\Theta_a \equiv (T_a - T_s)/(T_c - T_s)$ and $\Theta_L(X) \equiv [T_L(X) - T_s]/(T_c - T_s)$.

PERTURBATION ANALYSIS

Equations (19) and (20) with boundary conditions (21) and (22) are a set of nonlinear partial differential equations with nonlinear boundary conditions that could have been solved numerically on the basis of the finite difference method by iteration. However, since the value of ϵ in (19)–(22) is small, the mathematical problem can be simplified considerably by means of a perturbation technique. For this purpose we now assume that dependent variables are expanded in a power series of ϵ. Thus we have

$$P(X, Y) = \sum_{m=0}^{\infty} \epsilon^m P_m(X, Y) \tag{23a}$$

$$\Theta(X, Y) = \sum_{m=0}^{\infty} \epsilon^m \Theta_m(X, Y) \tag{23b}$$

$$\eta(X) = 1 + \sum_{m=1}^{\infty} \epsilon^m \eta_m(X) \tag{23c}$$

where $P_m(X, Y)$, $\Theta_m(X, Y)$, and $\eta_m(X)$ are perturbation functions to be determined. Substituting (23) into (19)–(22), making a Taylor series expansion on boundary conditions (21*d*), (21*e*), and (22*d*), and collecting terms of like power in ϵ, we have the following set of subproblems:

Zero-order approximations. The zero-order problem for P is given by

$$\frac{\partial^2 P_0}{\partial X^2} + \frac{\partial^2 P_0}{\partial Y^2} = 0 \tag{24}$$

with boundary conditions given by

$$P_0(0, Y) = 1 - Y \tag{25a}$$

$$P_0(L, Y) = 1 - Y \tag{25b}$$

$$\frac{\partial P_0}{\partial Y}(X, 0) = -1 \tag{25c}$$

$$P_0(X, 1) = 0 \tag{25d}$$

Solution to the zero-order problem for P is obviously given by

$$P_0(X, Y) = 1 - Y \tag{26}$$

which physically means the hydrostatic situation.

With the aid of (26) the zero-order problem for Θ is given by

$$\frac{\partial^2 \Theta_0}{\partial X^2} + \frac{\partial^2 \Theta_0}{\partial Y^2} = 0 \tag{27}$$

boundary conditions being given by

$$\Theta_0(0, Y) = 0 \tag{28a}$$

$$\Theta_0(L, Y) = 0 \tag{28b}$$

$$\Theta_0(X, 1) = \Theta_a \tag{28c}$$

$$\Theta_0(X, 0) = \Theta_L(X) \tag{28d}$$

Thus to the zero-order approximation, pressure is given by the hydrostatic pressure and temperature distribution is due to heat conduction; the fluid flow and heat transfer are decoupled in the zero-order approximation. Furthermore, (25*d*) and (28*c*) show that we have successfully transferred the boundary conditions at the unknown free surface to $Y = 1$.

First-order approximations. With the aid of (26) the first-order problem for P is given by

$$\frac{\partial^2 P_1}{\partial X^2} + \frac{\partial^2 P_1}{\partial Y^2} = \frac{\partial \Theta_0}{\partial Y} \tag{29}$$

where the right-hand side of (29) is known from the zero-order problem. The boundary conditions for P_1 are given by

$$P_1(0, Y) = 0 \tag{30a}$$

$$P_1(L, Y) = 0 \tag{30b}$$

$$\frac{\partial P_1}{\partial Y}(X, 1) = \Theta_a \tag{30c}$$

$$\frac{\partial P_1}{\partial Y}(X, 0) = \Theta_L(X) \tag{30d}$$

Once P_1 is determined, $\eta_1(X)$ is obtained from

$$\eta_1(X) = P_1(X, 1) \tag{30e}$$

which follows from substituting (23*a*) and (23*c*) into boundary condition (21*e*) and making a Taylor series expansion. Equation (30*e*) gives the influence of the geothermal heating on the shape of the free surface. Equations (29)–(30) show that the value of P_1, and consequently η_1, depends on the vertical temperature gradient in the medium as well as the prescribed temperature distribution on the impermeable surface. Thus to the first-order approximation the amount of upwelling of the water table, which is given by $\epsilon\eta_1$, depends on the amount of geothermal heating.

With the aid of (26) the first-order approximation for Θ is

$$\frac{\partial^2 \Theta_1}{\partial X^2} + \frac{\partial^2 \Theta_1}{\partial Y^2} = -D\left[\frac{\partial P_1}{\partial X}\frac{\partial \Theta_0}{\partial X} + \frac{\partial P_1}{\partial Y}\frac{\partial \Theta_0}{\partial Y} - \Theta_0 \frac{\partial \Theta_0}{\partial Y}\right] \tag{31}$$

boundary conditions being given by

$$\Theta_1(0, Y) = 0 \tag{32a}$$

$$\Theta_1(L, Y) = 0 \tag{32b}$$

$$\Theta_1(X, 0) = 0 \tag{32c}$$

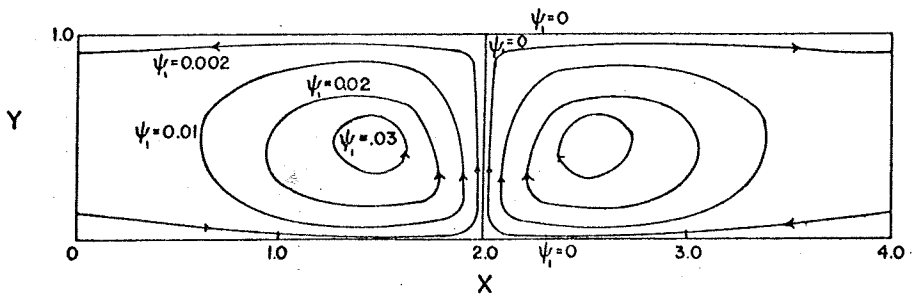

Fig. 2. Contours of first-order perturbation for stream function.

$$\Theta_1(X, 1) = -P_1(X, 1)\frac{\partial \Theta_0}{\partial Y}(X, 1) \qquad (32d)$$

An alternate formulation in terms of stream function is given by *Cheng and Lau* [1974]. The major advantages of the application of the perturbation method to the present problem are: (1) the problem becomes linear and the difficulty in the nonconvergence of iteration associated with the numerical solution of nonlinear finite difference equations does not exist, (2) the unknown position of the water table is explicitly determined from the first-order problem; thus the usual practice of iteration of the position of the water table is avoided, and (3) a clearer physical picture emerged with regard to the driving forces and the role played by various parameters in heat transfer and fluid flow characteristics in a geothermal reservoir.

Numerical Computations and Results

The governing equations for the zero- and first-order problems as given by (27)–(32) are the Laplace equation and Poisson equation, respectively, with nonhomogeneous boundary conditions. In principle they can be solved in closed form by the classical method of separation of variables. However, the numerical evaluation of the resultant expressions in terms of many double- and triple-Fourier series will be of dubious value because of its slow convergent rate. For this reason we resort to the numerical solution of these linear problems by the finite difference method.

The standard five-point formula of the finite difference method is applied to (27), (29), and (31). The resultant linear algebraic equations [*Cheng and Lau,* 1974] are solved by the Gauss-Seidel iteration method. The mesh size in both X and Y directions is chosen to be 0.1. The iteration process is terminated when the maximum value is changed by less than 0.1% of the previous cycle. Computation begins with the determination of Θ_0 from the finite difference equations corresponding to (27)–(28). After values of Θ_0 at all grid points are obtained, the partial differentiation of Θ_0 is computed by using the IBM scientific subroutine DET5. The partial derivatives of Θ_0 are then stored on disk and will be used for the determination of P_1 from the finite difference equations corresponding to (29)–(30). The differentiation of P_1 and the determination of Θ_1 from finite difference equations corresponding to (31)–(32) are done in the same manner.

The parameters for the present problem are the aspect ratio L, perturbation parameter ϵ, and the discharge number D. Since the purpose of this study is to have a qualitative understanding of the physical processes involved, the values of the parameters are arbitrarily chosen to be $L = 4$ and $\epsilon = 0.1$ with two different values of D at 50 and 500. The surface temperatures of the impermeable wall are arbitrarily chosen to be:

Case 1

$$\Theta_L = \exp\left[-\left(\frac{X - 2.0}{0.5}\right)^2\right]$$

with a maximum temperature at $X = 2.0$,

Case 2

$$\Theta_L = \exp\left[-\left(\frac{X - 0.5}{0.5}\right)^2\right]$$

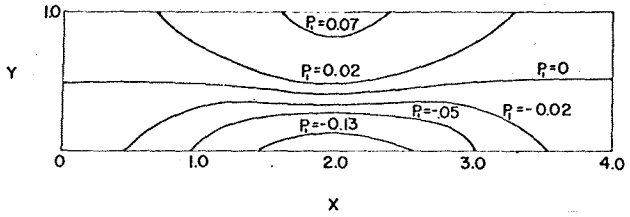

Fig. 3*a*. Contours of first-order perturbation function for pressure.

with a maximum temperature at $X = 0.5$,

Case 3

$$\Theta_L = \exp\left[-\left(\frac{X - 0.5}{0.1}\right)^2\right]$$

with a maximum temperature at $X = 0.5$. Comparison of the numerical results for case 1 (maximum temperature at $X = 2.0$) and case 2 (maximum temperature at $X = 0.5$) will show the effect of the location of heat source, whereas the comparison of results for case 2 (a broad heat source) and case 3 (a narrow heat source) will show the effect of the size of the heat source.

Figure 2 shows the contour of the first-order perturbation of dimensionless stream function (normalized with respect to the quantity $\rho_s ghK/\mu$) ψ_1 for case 1. As is shown in the figure, the fluid particles begin to rise as they approach the point of maximum surface temperature because the density of the fluid becomes smaller as its temperature rises. As the fluid particles rise to a colder region they begin to lose heat and will begin their descending paths when the density becomes the same as that of the surrounding fluid. Since $\psi_0 = 0$ and $\psi = \epsilon\psi_1$ to the first-order approximation, the amount of convective current can be estimated by the difference in the values of the stream function $\epsilon\psi_1$.

Figure 3*a* shows the contours of the first-order pressure function P_1 for case 1. As is shown in (29)–(30), P_1 is induced by the nonisothermal temperature distribution on the boundary and the vertical temperature gradient. The values of P_1 are independent of D, being negative in the lower portion of the aquifer and having a minimum value at the point of maximum surface temperature. On the other hand, the values of P_1 are positive in the upper portion of the aquifer with a maximum value at the point (2, 1). Thus the fluid particles are drawn inward in the lower portion of the aquifer and are forced to move toward the ocean in the upper portion of the aquifer. Figure 3*b* shows the pressure contours for case 1 with $\epsilon = 0.1$ and for all values of D. The fact that the pressure contours are almost horizontal indicates that the pressure in an unconfined geothermal reservoir can be approximated by hydrostatic pressure.

Figure 4*a* shows the contours of the zero-order perturbation function for temperature for case 1. In the zero-order approximation, heat is transferred by conduction as a result of

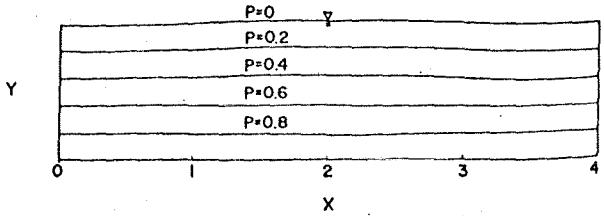

Fig. 3*b*. Pressure contours for case 1.

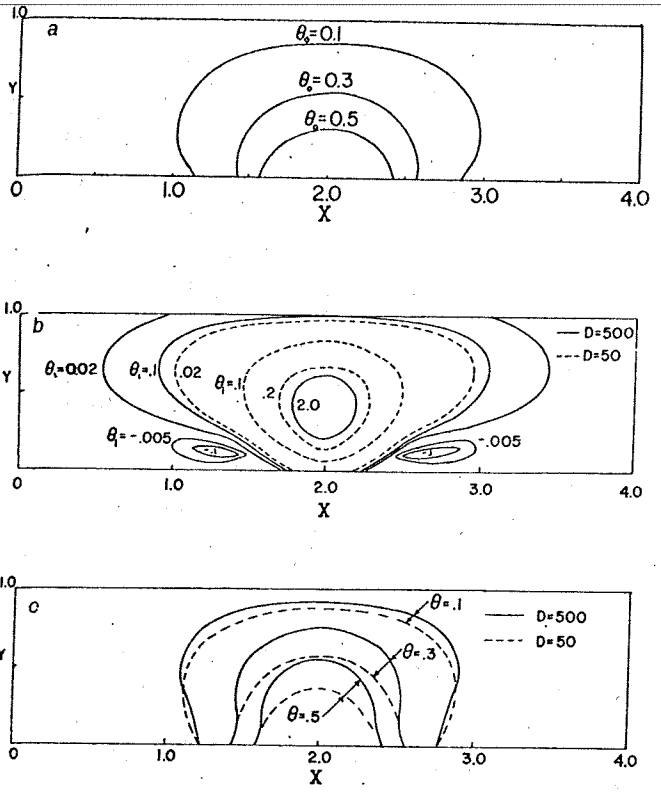

Fig. 4. (*a*) Contours of zero-order perturbation function for temperature. (*b*) Effect of discharge number on the contours of first-order perturbation function of temperature. (*c*) Effect of discharge number on temperature contours for case 1.

nonisothermal temperature on the boundary. Thus the value of Θ_0 is independent of D. Figure 4*b* shows the contours of first-order perturbation temperature Θ_1, the temperature correction being due to convective current. As is expected, the convective current helps to diffuse heat, and consequently, the contours of temperature are pushed further away from the heat source as the value of D is increased. The maximum value of Θ_1 is in a region that is slightly above the point of maximum geothermal heating. The regions of negative value of Θ_1 indicate the inward movement of cold water from the ocean. The effect of discharge number on temperature contours for $\epsilon = 0.1$ is shown in Figure 4*c*. Comparison of Figures 4*a* and 4*c* shows that the difference between temperature contours Θ_0 and Θ_1 is small for $D = 50$; thus it is indicated that heat transfer by conduction is predominant for small value of D. There is a significant difference in temperature contours for $D = 500$, especially in the region of maximum heating, which suggests that there is a strong convection current there.

The effects of discharge number, the location of the heat source, and the size of the heat source on the horizontal temperature distribution are shown in Figures 5*a*, 5*b*, and 5*c*. The prescribed temperature distribution of the impermeable rock is indicated by $Y = 0$. It is interesting to note that, with the exception of a narrow heat source, the width of the temperature profiles at lower elevations fall within the temperature profile at $Y = 0$, thus it is indicated that the lateral diffusion of heat by convection is not very effective. As is expected, temperature is higher for higher values of D at the same location (Figure 5*a*). To show the effect of location on the horizontal temperature distribution, results for cases 1 and 2 with $D = 500$ and $\epsilon = 0.1$ are plotted in Figure 5*b*. When the heat source is near the ocean as in case 2, although there is a

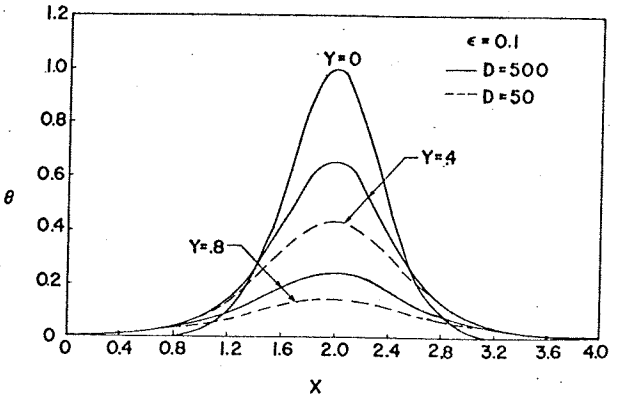

Fig. 5*a*. Effect of discharge number on the horizontal temperature distribution for case 1.

significant drop in temperature on the ocean side of the heat source due to inward movement of cold seawater, temperature on the other side of the heat source is only slightly affected. To show the effect of size of the heat source on the horizontal temperature distribution, results for case 2 (a broad heat source) and case 3 (a narrow heat source) with $D = 500$ and $\epsilon = 0.1$ are plotted in Figure 5*c*. It is shown in this figure that temperature is higher for a broad heat source than for a narrow heat source.

The effect of discharge number on vertical temperature profiles is shown in Figure 6*a* (case 1) and in Figure 6*b* (case 2). For locations directly above the point of maximum surface temperature (i.e., at $X = 2$ in Figure 6*a* and $X = 0.5$ in Figure 6*b*), temperature is higher for a higher value of D. Similar behavior exists in the upper portion of the aquifer. However, in the lower portion of the aquifer, temperature decreases as the value of D is increased. This result is due to the inflow of colder seawater in the lower portion of the aquifer and the outflow of warmer seawater in the upper portion of the aquifer. The behavior is more pronounced for case 2 (Figure 6*b*) than case 1 (Figure 6*a*), since the amount of inflow of cold seawater is larger for case 2. To show the effect of location of the heat source on vertical temperature profiles, data for Figures 6*a* and 6*b* with $D = 500$ and $\epsilon = 0.1$ are replotted in Figure 6*c*. It is shown that the effect of location on vertical temperature profiles is small for positions directly above the point of maximum surface temperature ($X = 2$ and 0.5). For the vertical positions 0.4 unit away from the point of maximum surface temperature, comparison of the curve of $X = 1.6$ for case 1 to that of $X = 0.1$ for case 2 shows that there is a significant drop

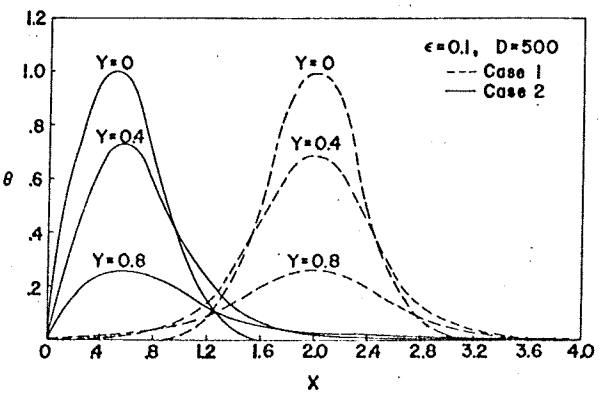

Fig. 5*b*. Effect of the location of heat source on the horizontal temperature distribution.

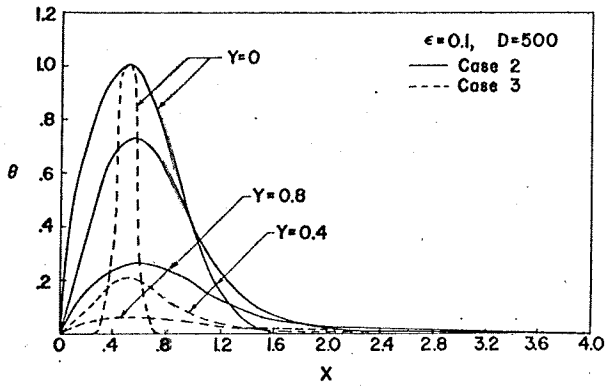

Fig. 5c. Effect of the size of the heat source on the horizontal temperature distribution.

in temperature at the ocean side of the heat source. Similar comparison of the curves $X = 2.4$ (for case 1) and $X = 0.9$ (for case 2) indicates that the temperature drop is small at the other side of the heat source. The effect of the size of the heat source on vertical temperature profiles for $D = 500$ and $\epsilon = 0.1$ is shown in Figure 6d. It is shown that there is a significant drop in temperature if the size of the heat source decreases.

Figure 7 shows the effect of location and the size of heat source on η_1, the first-order perturbation function for the shape of the water table. To the first-order approximation the upwelling of the water table is given by $\epsilon\eta_1$ and is independent of D. The amount of upwelling depends on the vertical temperature gradient of the porous medium and the temperature distribution of the impermeable surface. The size and the location of the heat source have a strong influence on the amount of upwelling of the water table. The maximum value of η_1 is approximately 0.08 at $X = 2$ for case 1 (Figure 7, top). For a heat source near the ocean (Figure 7, bottom) it is interesting to note that the location of maximum water table height is not necessarily located directly above the point of maximum temperature of the impermeable surface. In fact, the position of maximum value of η_1 moves inland as the size of the heat source is increased.

Concluding Remarks

A parametric study has been conducted to investigate the effects of various parameters on the movement of seawater, the upwelling of the water table, and the pressure and temperature distributions in a geothermal reservoir. It has been found to the first-order approximation that (1) the pressure in the unconfined geothermal reservoir is almost hydrostatic, (2) the flow rate of seawater depends only on the horizontal temperature gradient of the reservoir, (3) although there is some decrease in temperature distribution in the lower portion of the aquifer in a small region near the ocean as a result of inflow of cold water, the water also acts as a heat carrier in the rest of the aquifer, (4) the convection of heat is more efficient vertically than horizontally, (5) the size of the geothermal source has an important effect on the temperature distribution in the reservoir, (6) the location of the heat source will have some effect on the temperature distribution in the region near the ocean; its effect on the temperature of the rest of the

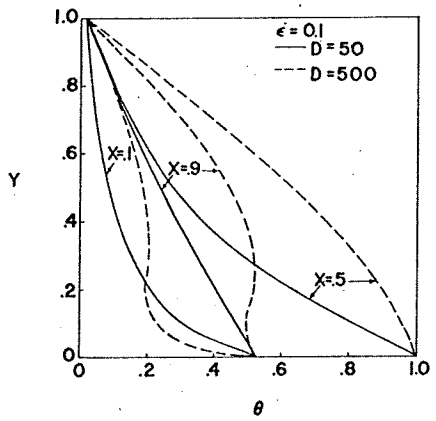

Fig. 6b. Effect of discharge number on vertical temperature profiles for case 2.

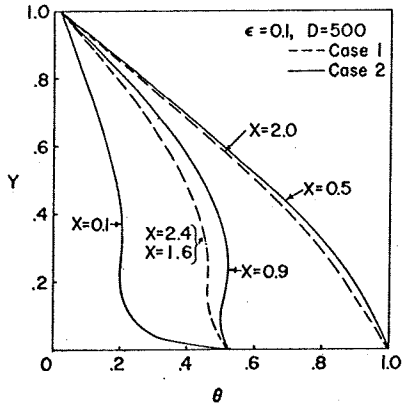

Fig. 6c. Effect of the location of the heat source on vertical temperature profiles.

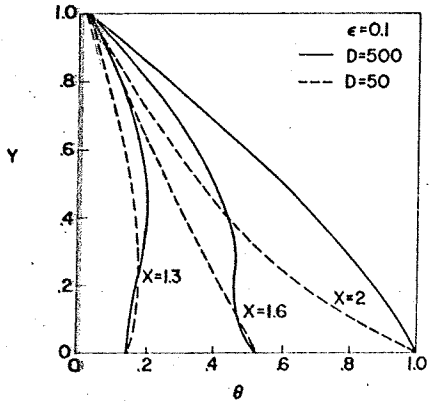

Fig. 6a. Effect of discharge number on vertical temperature profiles for case 1.

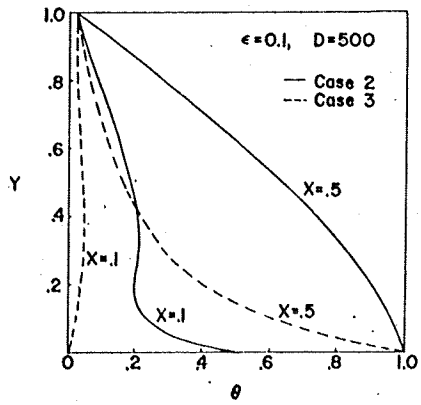

Fig. 6d. Effect of the size of the heat source on vertical temperature profiles.

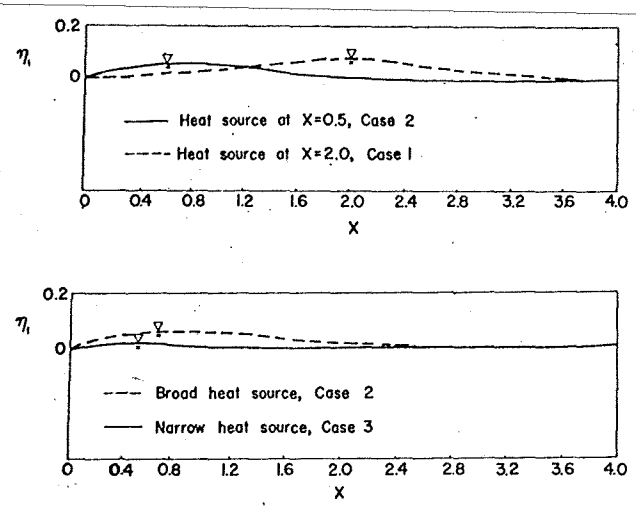

Fig. 7. (Top) Effect of the location of the heat source on the first-order perturbation function for the upwelling of water table. (Bottom) Effect of the size of the heat source on the first-order perturbation function for the upwelling of water table.

aquifer is small, (7) the discharge number has a strong effect on temperature distribution in the aquifer, and (8) there is a noticeable upwelling of the water table at the location directly above the heat source; the amount of upwelling depends on the vertical temperature gradient of the porous medium and the prescribed temperature of the impermeable surface. The upwelling of the water table as a result of geothermal heating is predicted analytically for the first time.

Acknowledgments. The authors wish to thank H. J. Ramey, Jr., of Stanford University for suggesting the problem and his encouragement throughout this work. Thanks are also due to P. C. Yuen, B. H. Chen, L. S. Lau, W. Brigham, and J. F. Mink for helpful discussion, to G. Nishiura for assistance in the numerical computation, to M. Nathenson and the anonymous reviewer for constructive suggestions that led to the improvement of the manuscript. This work was supported by the Research Applied to National Needs Program, National Science Foundation under grant GI-38319.

REFERENCES

Bories, S. A., and M. A. Combarnous, Natural convection in a sloping porous layer, *J. Fluid Mech., 57,* 63–70, 1973.

Chan, B. K. C., C. M. Ivey, and J. M. Barry, Natural convection in enclosed porous media with rectangular boundaries, *J. Heat Transfer, 2,* 21–27, 1970.

Cheng, P., and K. H. Lau, Steady state free convection in an unconfined geothermal reservoir, *Tech. Rep. 2,* Hawaii Geothermal Project, College of Eng., Univ. of Hawaii, Honolulu, March 1, 1974.

Combarnous, M. A., and P. Bia, Combined free and forced convection in porous media, *Soc. Petrol. Eng. J., 4,* 399–405, 1971.

Donaldson, I. G., Temperature gradients in the upper layers of the earth's crust due to convective water flows, *J. Geophys. Res., 67,* 3449–3459, 1962.

Elder, J. W., Steady free convection in a porous medium heated from below, *J. Fluid Mech., 27,* 29–48, 1967*a*.

Elder, J. W., Transient convection in a porous medium, *J. Fluid Mech., 27,* 609–623, 1967*b*.

Henry, H. R., and F. A. Kohout, Circulation patterns of saline groundwater affected by geothermal heating—As related to waste disposal, *Underground Waste Manage. Environ. Implications, 18,* 202–221, 1973.

Holst, P. H., and K. Aziz, A theoretical and experimental study of natural convection in a confined porous medium, *Can. J. Chem. Eng., 50,* 232–241, 1972*a*.

Holst, P. H., and K. Aziz, Transient three-dimensional natural convection in confined porous media, *Int. J. Heat Mass Transfer, 15,* 73–90, 1972*b*.

Horton, C. W., and F. T. Rogers, Jr., Convective currents in a porous medium, *J. Appl. Phys., 16,* 367–370, 1945.

Katto, Y., and T. Masuoka, Criterion for the onset of convective flow in a fluid in a porous medium, *Int. J. Heat Mass Transfer, 10,* 297–309, 1967.

Lapwood, E. R., Convection of a fluid in a porous medium, *Proc. Cambridge Phil. Soc., 44,* 508–521, 1948.

Prats, M., The effect of horizontal fluid flow in thermally induced convection currents in porous media, *J. Geophys. Res., 71,* 4835–4838, 1966.

Wooding, R. A., Steady state free thermal convection of liquid in a saturated permeable medium, *J. Fluid Mech., 2,* 273–285, 1957.

Wooding, R. A., Rayleigh instability of a thermal boundary layer in flow through a porous medium, *J. Fluid Mech., 9,* 183–192, 1960.

(Received April 22, 1974;
revised July 15, 1974;
accepted July 24, 1974.)